JACS
JOURNAL OF THE AMERICAN CHEMICAL SOCIETY

COMMUNICATION

pubs.acs.org/JACS

Observations of Shape-Dependent Hydrogen Uptake Trajectories from Single Nanocrystals

Ming L. Tang,[†,‡] Na Liu,[†,‡] Jennifer A. Dionne,[†,§] and A. Paul Alivisatos*[,†]

[†]Materials Sciences Division, Lawrence Berkeley National Laboratory, and Department of Chemistry, University of California, Berkeley California 94720, United States

Supporting Information

ABSTRACT: In this work, H_2 absorption and desorption in faceted, crystalline Au/Pd core/shell nanocrystals and their interaction with a SiO_x/Si support were studied at the single-particle level. Dark-field microscopy was used to monitor the changing optical properties of these Au/Pd nanoparticles (NPs) upon exposure to H_2 as reversible H_2 uptake from the Pd shell proceeded. Analysis of the heterogeneous ensemble of NPs revealed the H_2 uptake trajectory of each nanocrystal to be shape-dependent. Differences in particle uptake trajectories were observed for individual particles with different shapes, faceting, and Pd shell thickness. In addition to palladium hydride formation, the single-particle trajectories were able to decipher specific instances where palladium silicide formation and Au/Pd interdiffusion occurred and helped us determine that this was more frequently seen in those particles within an ensemble having thicker Pd shells. This noninvasive, plasmonic-based direct sensing technique shows the importance of single-particle experiments in catalytically active systems and provides a foundation for studying more complex catalytic processes in inhomogeneous NP systems.

There are many examples where the activity of catalytic inorganic nanoparticles (NPs) is known to depend strongly upon their size[1,2] and shape,[3,4] the precise nature of their faceting,[5,6] and their interaction with any support.[7,8] It is also well-known that all of these parameters frequently change during the continued use of a catalyst.[9,10] Furthermore, catalytic systems are commonly inhomogeneous with respect to all of these variables, making it very challenging to understand and control the factors that lead to enhanced catalyst performance.

For these reasons, there is tremendous interest in harnessing the methods of single-particle optical spectroscopy to observe the trajectories of catalytic events for individual NPs and in correlating these trajectories with results obtained using other structural and chemical probes. For instance, Chen and co-workers used bright organic chromophores as the product of a turnover event and then employed the methods of single-molecule luminescence to monitor single-particle catalyst trajectories.[11] Kasemo and co-workers laid the groundwork for the use of plasmonic sensing for the indirect detection of catalytic events such as H_2 storage in Pd[12] and CO and H_2 oxidation on Pt[13] at the ensemble level. They showed that catalytic changes that alter the dielectric permittivity in the environment of a nearby metallic particle can be detected using a plasmonic platform with a large extinction cross section, providing an optical method to detect the catalysis indirectly. We recently extended their work by employing electron beam lithography to prepare a model system of Au antennas near Pd particles with exceptionally good homogeneity and showed that plasmonic light scattering can be used to detect H_2 uptake at the single-particle level.[14]

In this paper, we demonstrate the observation of single-particle H_2 uptake trajectories from individual nanocrystals (NCs) of Au coated with a thin layer of Pd using dark-field spectroscopy. We show that it is possible to dissect the behavior of an inhomogeneous NP ensemble and detect significant differences between the types of trajectory for particles of differing shape that are mixed together.

Here we examined the chemically important case where the NPs are inhomogeneous and change during the reaction under study. We investigated a direct sensing platform involving catalytically active Au/Pd core/shell NCs with sizes of 100−200 nm at room temperature (RT). H_2 uptake by these NCs was studied by monitoring the change in optical properties as PdH was formed. H_2 uptake is an excellent system for plasmonic sensing of catalysis because many catalytic events on a single particle produce an integrated effect upon the dielectric constant of the NP, as demonstrated by Kasemo and co-workers in their indirect sensing studies on the ensemble. The reaction involves the chemisorption of H_2 on a Pd surface, its nearly barrierless dissociation, and the diffusion of atomic hydrogen into the bulk material to form PdH. The Au NC reports on the amount of hydrogen stored in its epitaxially grown Pd shell through the change in refractive index of the Pd shell. This is monitored by measuring the scattering spectra of single particles that arise from their localized surface plasmon resonances (LSPRs). The scattering spectrum of each particle is recorded in situ at varying H_2 partial pressures (P_{H_2}) and correlated with the NC geometry by scanning electron microscopy (SEM). These are the first single-particle H_2 storage experiments that employ a *direct* plasmonic sensing scheme, where hydride formation and particle evolution over time are detected optically in situ.

For this experiment, we employed a synthesis known to yield a sample of high-quality NCs with significant sample inhomogeneity. The colloidal synthesis of Au@Pd NPs was adapted from a report by Lee et al.[15] Au^{3+}(aq) and Pd^{2+}(aq) in a 3:1 ratio (or 2:1 for NPs with a thicker shell) were dissolved

Received: April 7, 2011
Published: July 27, 2011

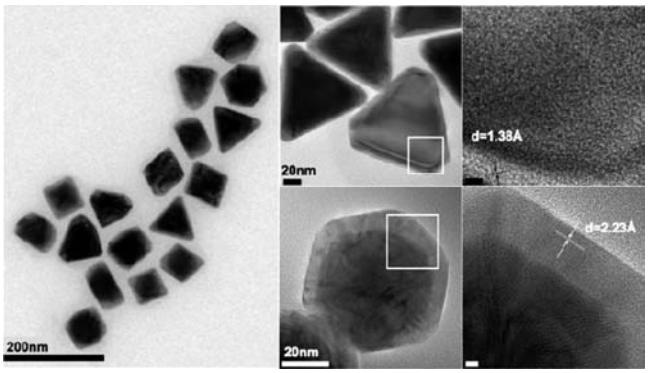

Figure 1. (left) TEM image of the Au/Pd core/shell NCs. (top right) HRTEM image of the square outlined on the triangular plate (top middle). The shell shows a *d* spacing of 1.38 Å correspondin to Pd{220}. (bottom right) HRTEM image corresponding to the square on the icosahedron (bottom middle). The lattice spacing of 2.23 Å in the shell matches that of Pd{111}. Bottom-right scale bar: 2 nm.

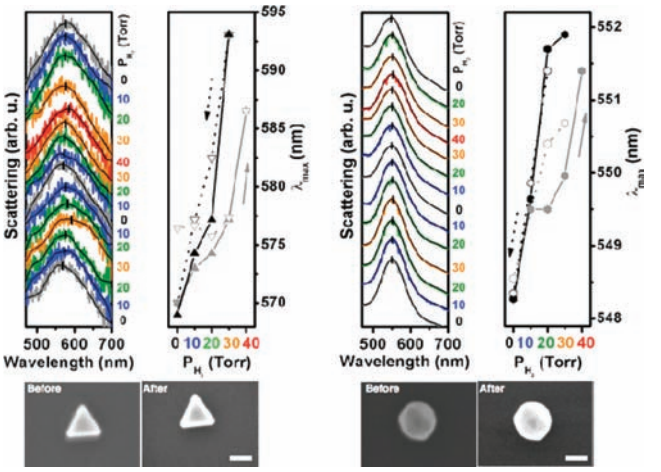

Figure 2. Scattering spectra of a Au/Pd core/shell triangular plate (left) and icosahedron (right). Two cycles of increasing and decreasing P_{H_2} (first cycle, black; second cycle, gray) are shown. Absorption: solid triangles (left) and hexagons (right). Desorption: open triangles (left) and hexagons (right). The total red shift was ~25 nm for the triangular plate but <4 nm for the icosahedron. The scale bars in the SEM images represent 100 nm. All measurements were performed at RT.

in water with cetyltrimethylammonium chloride, placed in a Parr bomb at 90 °C for 2 days, and then held at 115 °C for another day [see the Supporting Information (SI)]. Initial nucleation and growth of small Au particles was followed by epitaxial deposition of the Pd shell, which was encouraged by the slow growth conditions. Figure 1 shows a transmission electron microscopy (TEM) image of the core/shell NPs as a mixture of triangular plates, decahedrons, and icosahedrons. High-resolution TEM (HRTEM) studies of individual NPs showed that the cores of these particles were composed mainly of Au, while the shells were made of Pd. For example, the HRTEM image in Figure 1 shows a lattice spacing of 2.23 Å in the shell that corresponds to the {111} planes of face-centered cubic Pd. The UV−vis spectrum of these NCs in water is shown in Figure S1 in the SI. After synthesis, the particles were cleaned three times and redispersed in deionized water. The particles were then drop-cast onto an aqua regia-cleaned, native oxide-coated p-type ⟨100⟩ Si wafer for imaging and chemical reaction.

Single-particle scattering spectra were collected using dark-field microscopy in reflection mode with a long-working-distance objective (50×, NA 0.55) through a thin fused silica window. The long working distance enabled single-particle studies in an air-free stainless steel cell that allowed precise control over P_{H_2} (see the SI). The scattering spectra of individual NCs were correlated with their structures using SEM by matching their relative spatial distributions in the camera to the exact same arrangement on the SiO_x/Si substrate. These NCs were allowed to equilibrate in dry N_2 overnight before measurements commenced. Mass flow controllers were used to define P_{H_2} by varying the relative flow rates of the ultrahigh-purity N_2 and H_2 over the sample at RT. More than 50 single particles were measured.

NCs with different shapes within the same sample showed remarkably different light scattering trajectories as a function of H_2 uptake. Reversible LSPR shifts correlated with P_{H_2} (and hence the hydrogen stored in the Au/Pd core/shell NCs) are shown in Figure 2 for a single triangular plate and a single icosahedron. As PdH is formed, the refractive index of the Pd shell changes, thus allowing spectral characterization of this transition. A red shift corresponding to H_2 adsorption and a blue shift upon desorption was seen. Simulated spectra for these spectral changes (Figure S2) were obtained using the dielectric permittivities of bulk Pd and PdH.[16,17] At P_{H_2} = 30−40 Torr, the triangular plate showed shifts of 25 nm, which were much larger than the shifts of <4 nm for the icosahedron. This occurred because induced electromagnetic fields are more confined in metallic nanostructures with sharper corners or edges, giving rise to a higher sensitivity. After two cycles of H_2 absorption and desorption, the spectra of these single NCs did not return to their starting spectral positions. This hysteresis in the LSPR is attributed to the residual H atoms on the subsurface sites of Pd that cannot be removed at RT.[18,19] It has been shown that subsurface hydride and chemisorbed hydrogen are stable at RT.[20,21] Control experiments showed no change in the LSPR of pure Au NCs with increasing P_{H_2} (Figure S3). This is expected for Au, which is inert toward H_2.

Decahedral core/shell NPs synthesized in the same batch showed a qualitatively different behavior in comparison with the icosahedra and the triangular plates. The decahedral NPs consistently showed an initial blue shift (rather than a red shift) upon H_2 uptake (Figure 3). This behavior was observed for all of the decahedrons measured. Upon careful examination of the TEM images of the inhomogeneous sample, we observed that the thickness of the Pd shell was uniformly thicker for the decahedral NPs than for the triangular- and hexagonal-shaped ones. Although all of the shapes formed in a single reaction medium, the deposition kinetics differed depending upon the faceting. We were able to demonstrate that the initial blue shift of the plasmon upon H_2 exposure was correlated with the thickness of the Pd shell by preparing another sample with thicker Pd shells on the NPs. These NPs also displayed a blue shift upon initial H_2 exposure. For example, in the case of the hexagonal plate in Figure 3, very large blue shifts on the order of 30 nm were observed when P_{H_2} was increased. These dramatic LSPR shifts were also seen as P_{H_2} was cycled again, although no obvious morphological changes were observed in the SEM micrographs taken before and after H_2 exposure.

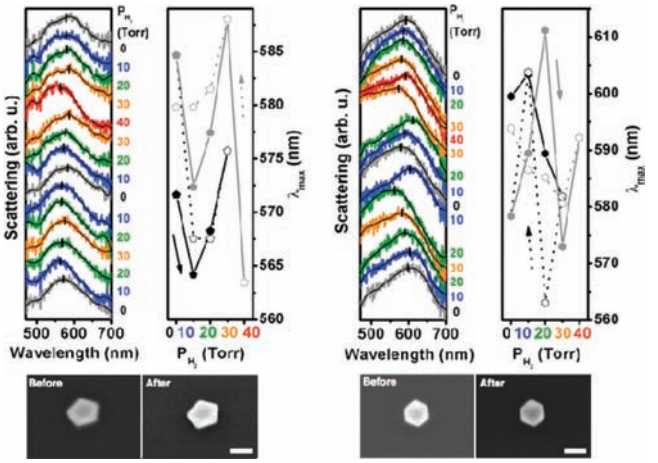

Figure 3. Scattering spectra of a Au/Pd core/shell decahedron (left) and a hexagonal plate with a thicker Pd shell (right). Two cycles of increasing and decreasing P_{H_2} (first cycle, black; second cycle, gray) are shown. Absorption: solid pentagons (left) and hexagons (right). Desorption: open pentagons (left) and hexagons (right). The spectral shift was <20 nm for the decahedron and >30 nm for the hexagonal plate. The scale bars in the SEM images represent 100 nm. All of the measurements were performed at RT.

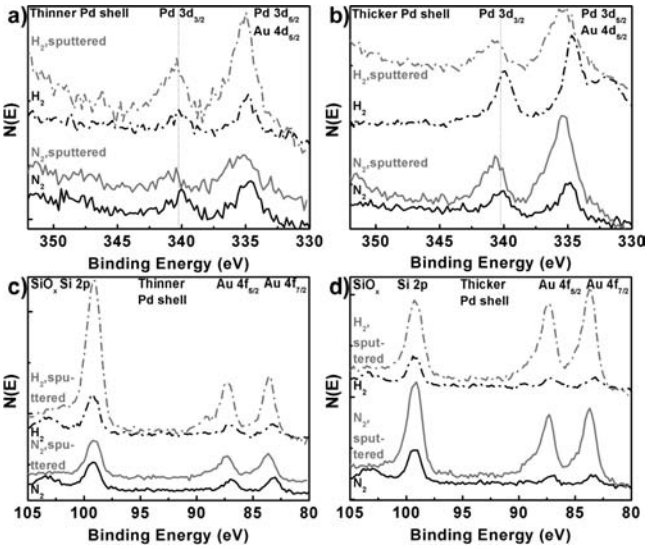

Figure 4. XPS data for Au/Pd core/shell NPs exposed either to N_2 only or to two cycles of P_{H_2} for particles with (a, c) thinner and (b, d) thicker Pd shells. At the top surface of the NPs, only ones with thicker shells (b) showed Au/Pd interdiffusion after H_2 exposure (decrease of 0.2 eV in BE for Pd $3d_{3/2}$), while all of the NPs regardless of shell thickness showed Au and Pd silicide formation after sputtering (an increase of 0.6−1.0 eV in BE for all Au/Pd peaks). Black, XPS of the top surface of the NPs; gray, XPS of NPs sputtered ∼50 nm. Solid lines, control experiment with particles exposed only to N_2; dot-dashed lines, particles exposed to two cycles of increasing and decreasing P_{H_2}.

Plasmon scattering simulations were unable to account for the blue shift of the LSPR upon H_2 uptake when only the presence of Pd and PdH were considered, even in the presence of substantial strain at the PdH−Au interface, or further in the case where the PdH breaks up into domains. We were therefore forced to conclude that there was an additional chemical transformation that took place upon H_2 exposure in the specific case where the Pd shell was quite thick. There were two possible transformations that could account for the blue shift: Au/Pd interdiffusion and silicide formation.

At RT, the diffusion coefficient (D) for bulk Au/Pd is 10^{-20} cm^2/s, which indicates that diffusion is too slow to be significant over the course of this measurement. However, enhanced diffusion across grain boundaries increases D for Au/Pd by several orders of magnitude.[22−26] The stress associated with the expansion of the Pd shell upon H_2 absorption would create more grain boundaries or defects in a thicker shell than a thinner shell. Furthermore, the interdiffusion of Au and Pd may result in a blue shift of the LSPR because it essentially has an effect similar to decreasing the Au particle size. X-ray photoelectron spectroscopy (XPS) experiments (Figure 4b) showed a decrease in binding energy (BE) of ∼0.2 eV for the Pd $3d_{3/2}$ peak after H_2 exposure, in line with reports of Au/Pd interdiffusion,[27−31] as Pd and Au gain d and s/p electrons respectively. Au/Pd interdiffusion has been observed at RT by Kaszkur[32] using X-ray diffraction of nanocrystalline Pd/Au supported on silica, where Au segregation to the surface was seen when the sample was pulsed with H_2 in a flow of Ar at RT.

Support interactions must also be considered carefully. Reaction of the NP with silicon from the substrate to form a palladium silicide may also account for the *observed initial blue shift* and is consistent with several prior observations.[10,33−36] A blue shift of the LSPR as Pd_2Si is formed can be clearly predicted from electromagnetic calculations and the values of the dielectric constants.[37] Figure S4 shows calculations that pertain directly to the hexagonal plate in Figure 3. The formation of palladium silicide is known to enhance certain catalytic reactions. For example, Pd silicide formation noticeably increases the selectivity for the isomerization of neopentane.[38] It is possible for Si to diffuse through pinholes in the ultrathin surface oxide and react with Pd. Avci and co-workers documented this with XPS depth profiling of plasma-deposited PdAu on 45−50 Å Si oxide on Si. They observed the formation of both Au and Pd silicides while the samples were kept at RT during deposition and analysis.[39] Diffusion of Si occurs through the thin SiO_x to form metallic silicides. When we performed similar XPS depth profiling (Figure 4), we found that Au and Pd silicides formed in all the samples, regardless of exposure to N_2 or H_2. However, silicide formation was observed only midway through the >100 nm NP (i.e., after sputtering ∼50 nm away). XPS of the as-deposited NPs, with which only the NP surface could be investigated, showed classic metallic Au/Pd peaks for NPs with thinner Pd shells (Figure 4c) and Pd peaks shifted to lower BE for thicker Pd shells (Figure 4b) that can be assigned to Au/Pd interdiffusion. However, we note that XPS is an ensemble-based measurement that averages over all of the particles present. The fact that the NPs in Figure 2 did not show a blue shift with increasing P_{H_2} implies either that those particles exhibited neither Au/Pd interdiffusion nor silicide formation or alternatively that such chemical reactions occurred on a much smaller scale, producing effects on the LSPR that were too small to be observed. The latter was supported by plasmon scattering simulations indicating that there is no change in the LSPR if the thickness of the Pd silicide shell is <2 nm. The LSPR is a very sensitive probe of such interactions when the dielectric permittivity of the metal is modified sufficiently by these chemical or structural changes.

A summary of the results for the 50 particles measured across different experiments is given in Figure S5. With increasing P_{H_2}, a red shift was observed when only PdH was formed, as seen for 60% of the NPs; however, 20% showed an initial blue shift, which can be

attributed to Au/Pd interdiffusion or Au/Pd silicide formation. The remaining 20% did not show an LSPR shift, perhaps because both of these processes occurred simultaneously or the particles scattered too weakly for a change in the LSPR to be measured.

To conclude, we have demonstrated that H_2 storage and metal support interactions can be studied at a single-particle level. When colloidally synthesized Au/Pd core/shell NCs are used in a direct sensing platform, the change in the optical properties of the metallic NCs is correlated with the change in refractive index of the shell as hydride or silicide formation occurs. These noninvasive single-particle LSPR measurements were conducted under catalytically relevant conditions, without the expense and need for ultrahigh vacuum associated with conventional surface-science characterization techniques. The importance of single-particle studies is made clear by the study of a sample in which Pd-coated Au NPs with many different shapes were present simultaneously. While the triangular plates and icosahedrons showed LSPR shifts consistent with the bulk dielectric function of palladium hydride, the decahedrons showed an initial blue shift due either to palladium silicide formation or Au/Pd interdiffusion. Ensemble studies might have shown that this blue shift and the chemical transformation of the particles occurred in samples with greater shell thickness but would never have revealed the mixed response from NPs with different shapes. Ensemble-based experiments that average over properties of the entire system mask the hidden subtleties of individual particles.

■ ASSOCIATED CONTENT

Supporting Information. Experimental procedures and Figures S1−S5. This material is available free of charge via the Internet at http://pubs.acs.org.

■ AUTHOR INFORMATION

Corresponding Author
alivis@berkeley.edu

Present Addresses
[§]Department of Materials Science and Engineering, Stanford University, Stanford, CA 94305.

Author Contributions
[‡]These authors contributed equally.

■ ACKNOWLEDGMENT

The authors thank Dr. Yimin Li and Prof. Gabor A. Somorjai for valuable discussions and close reading of this manuscript. We thank David C. Grauer for performing the XPS sputtering experiments. This work was supported by the grant "A Synergistic Approach to the Development of New Classes of Hydrogen Storage Materials" from the U.S. Department of Energy (DE-AC03-76SF00098). Chemicals were procured through the Plasmonic-Enhanced Catalysis Project of the Air Force Office of Science Research (Award FA9550-10-1-0504). SEM and XPS studies were performed at the Imaging and Manipulation Facility at the Molecular Foundry, and TEM work was done at the National Center for Electron Microscopy at the Lawrence Berkeley National Laboratory, supported by the U.S. Department of Energy, Office of Science, Office of Basic Energy Sciences, Division of Materials Sciences and Engineering (Contract DE-AC02-05CH11231).

■ REFERENCES

(1) Valden, M.; Lai, X.; Goodman, D. W. *Science* **1998**, *281*, 1647.
(2) Somorjai, G. A.; Li, Y. *Introduction to Surface Chemistry and Catalysis*, 2nd ed.; Wiley: Hoboken, NJ, 2010.
(3) Boudart, M. *J. Mol. Catal.* **1985**, *30*, 27.
(4) Dumesic, J. A.; Topsoe, H.; Khammouma, S.; Boudart, M. *J. Catal.* **1975**, *37*, 503.
(5) Bratlie, K. M.; Lee, H.; Komvopoulos, K.; Yang, P. D.; Somorjai, G. A. *Nano Lett.* **2007**, *7*, 3097.
(6) Tsung, C. K.; Kuhn, J. N.; Huang, W. Y.; Aliaga, C.; Hung, L. I.; Somorjai, G. A.; Yang, P. D. *J. Am. Chem. Soc.* **2009**, *131*, 5816.
(7) Min, B. K.; Santra, A. K.; Goodman, D. W. *Catal. Today* **2003**, *85*, 113.
(8) Boudart, M.; Aldag, A. W.; Ptak, L. D.; Benson, J. E. *J. Catal.* **1968**, *11*, 35.
(9) Narayanan, R.; El-Sayed, M. A. *J. Am. Chem. Soc.* **2003**, *125*, 8340.
(10) Fu, Q.; Wagner, T. *Surf. Sci. Rep.* **2007**, *62*, 431.
(11) Xu, W. L.; Kong, J. S.; Yeh, Y. T. E.; Chen, P. *Nat. Mater.* **2008**, *7*, 992.
(12) Langhammer, C.; Larsson, E. M.; Kasemo, B.; Zoric, I. *Nano Lett.* **2010**, *10*, 3529.
(13) Larsson, E. M.; Langhammer, C.; Zoric, I.; Kasemo, B. *Science* **2009**, *326*, 1091.
(14) Liu, N.; Tang, M. L.; Hentschel, M.; Giessen, H.; Alivisatos, A. P. *Nat. Mater.* **2011**, *10*, 631.
(15) Lee, Y. W.; Kim, M.; Kim, Z. H.; Han, S. W. *J. Am. Chem. Soc.* **2009**, *131*, 17036.
(16) Vargas, W. E.; Rojas, I.; Azofeifa, D. E.; Clark, N. *Thin Solid Films* **2006**, *496*, 189.
(17) von Rottkay, K.; Rubin, M.; Duine, P. A. *J. Appl. Phys.* **1999**, *85*, 408.
(18) Pundt, A.; Kirchheim, R. *Annu. Rev. Mater. Res.* **2006**, *36*, 555.
(19) Boudart, M.; Hwang, H. S. *J. Catal.* **1975**, *39*, 44.
(20) Behm, R. J.; Christmann, K.; Ertl, G. *Surf. Sci.* **1980**, *99*, 320.
(21) Behm, R. J.; Penka, V.; Cattania, M. G.; Christmann, K.; Ertl, G. *J. Chem. Phys.* **1983**, *78*, 7486.
(22) Gossner, K.; Mizera, E. *J. Electroanal. Chem.* **1981**, *125*, 359.
(23) Hall, P. M.; Morabito, J. M.; Poate, J. M. *Thin Solid Films* **1976**, *33*, 107.
(24) Murakami, M.; Defontaine, D.; Fodor, J. *J. Appl. Phys.* **1976**, *47*, 2850.
(25) Poate, J. M.; Turner, P. A.; Debonte, W. J.; Yahalom, J. *J. Appl. Phys.* **1975**, *46*, 4275.
(26) Debonte, W. J.; Poate, J. M. *Thin Solid Films* **1975**, *25*, 441.
(27) Lee, Y. S.; Jeon, Y.; Chung, Y. D.; Lim, K. Y.; Whang, C. N.; Oh, S. J. *J. Korean Phys. Soc.* **2000**, *37*, 451.
(28) Nascente, P. A. P.; Decastro, S. G. C.; Landers, R.; Kleiman, G. G. *Phys. Rev. B* **1991**, *43*, 4659.
(29) Han, Y. F.; Zhong, Z. Y.; Ramesh, K.; Chen, F. X.; Chen, L. W.; White, T.; Tay, Q. L.; Yaakub, S. N.; Wang, Z. *J. Phys. Chem. C* **2007**, *111*, 8410.
(30) Yi, C. W.; Luo, K.; Wei, T.; Goodman, D. W. *J. Phys. Chem. B* **2005**, *109*, 18535.
(31) Sohn, Y.; Pradhan, D.; Leung, K. T. *ACS Nano* **2010**, *4*, 5111.
(32) Kaszkur, Z. *Phys. Chem. Chem. Phys.* **2004**, *6*, 193.
(33) Brunner, A. J.; Oelhafen, P.; Guntherodt, H. J. *Surf. Sci.* **1987**, *189*, 1122.
(34) Rubloff, G. W.; Ho, P. S.; Freeouf, J. F.; Lewis, J. E. *Phys. Rev. B* **1981**, *23*, 4183.
(35) Lamber, R.; Jaeger, N.; Schulzekloff, G. *J. Catal.* **1990**, *123*, 285.
(36) Schleich, B.; Schmeisser, D.; Gopel, W. *Surf. Sci.* **1987**, *191*, 367.
(37) Lue, J. T.; Chen, H. W.; Lew, S. I. *Phys. Rev. B* **1986**, *34*, 5438.
(38) Juszczyk, W.; Karpinski, Z. *J. Catal.* **1989**, *117*, 519.
(39) Yalcin, S.; Avci, R. *Appl. Surf. Sci.* **2003**, *214*, 319.